Remotely Sensed Water Quality in Qatari Coastal Waters Between 2002 and 2022

Cheng Xue, Chuanmin Hu, Jennifer P. Cannizzaro, Brian B. Barnes, Lin Qi, Jing Shi, Yuyuan Xie, Benjamin D. Jaffe, and David A. Palandro, *Member, IEEE*

***Abstract*—Over the past two decades, Qatar has undergone significant economic growth and development, yet little information is available on long-term trends in seawater quality around the Qatar Peninsula. This study analyzed spatiotemporal variations of remotely sensed optical water quality (OWQ) parameters in Qatari coastal waters between 2002 and 2022. These OWQ parameters, including chlorophyll-a concentration (Chla), turbidity (Turb), and Secchi disk depth (SDD), along with sea surface temperature, were derived from Moderate-resolution Imaging Spectroradiometer (MODIS)/Aqua observations after applying an optically shallow-water mask. Additionally, changes in floating algae scum density, an indicator of harmful algal blooms (HABs), were derived from MultiSpectral Instrument (MSI) observations. Strong nearshore–offshore gradients were generally observed for all OWQ parameters (multiannual mean Chla $\sim$ 0.6–3 mg m^{-3}; Turb $\sim$ 0.2–3 FNU; and SDD $\sim$ 5–12 m). SDD was typically greatest in late spring and summer when Chla and Turb were relatively low. OWQ variability in the main territorial sea was mainly driven by suspended sediments, while in the broader Exclusive Economic Zone was driven by algal blooms. HABs dominated by *Margalefidinium polykrikoides*, *Noctiluca scintillans*, and *Trichodesmium* spp. were frequently observed in deeper (>20 m) waters. Despite Qatar's massive economic development in recent years, declines in Chla and Turb and increased SDD were observed. Qatari coastal waters, however, are warming at a rate of 0.64 °C/decade, $\sim$2–3 times faster than neighboring Red Sea and Northern Arabian Sea waters, and $\sim$8 times faster than the global oceans. This thermal stress may pose future challenges for marine ecosystems and the services they provide.**

***Index Terms*—Long-term trend, Qatari coastal waters, remote sensing, water quality.**

I. Introduction

QATAR is a peninsular nation with surrounding sea waters representing approximately 14% of the Persian Gulf/Arabian Gulf (hereafter the Gulf) [1]. Like the most areas within the Gulf, seawater quality around Qatar has experienced significant biotic and abiotic pressures [2], [3], [4], [5], [6], [7]. For example, harmful algal blooms (HABs) occur frequently in the Gulf [2], [3], [8], [9]. An eight-month-long, widespread bloom of the toxic dinoflagellate *Margalefidinium* (previously *Cochlodinium*) *polykrikoides* extended over the north of Qatar and led to fish mortalities and closure of desalination plants during 2008 and 2009 [10]. Additionally, the waters around Qatar [11], [12] and the Gulf [8] have some of the highest average sea surface temperatures (SSTs) in the world. With global oceans warming at a rate of 0.08 °C/decade [13], increased temperature may alter the biogeochemistry of ocean waters. Also, when coupled with increased stratification, warmer waters can limit vertical mixing, preventing oxygen replenishment in bottom waters [6]. The horizontal extension of the near-bottom hypoxia zone is observed within the Gulf, and the affected area exceeded 7000 km^2 for Qatar [4], [14], [15]. Moreover, inputs from multiple industrial activities within the Gulf, such as oil and gas fields on/off the shore and desalination plants, may impact water quality [5], [6]. Qatar is wholly dependent on desalinated seawater for its municipal water consumption (i.e., irrigation and drinking) [16]. Because changes in seawater quality can impact desalination efficiencies [5], [6], [17] and the continuous disposal of brine water from desalination plants into the Gulf may adversely affect water quality, the associated marine ecosystems [6], [18], [19], and the services those ecosystems provide [20], it is critical to monitor when and how seawater quality changes.

Despite the importance of the seawater desalination to the State of Qatar, change in seawater quality around Qatar is relatively understudied. To date, only a handful of papers have used *in situ* measurements to study Qatari coastal waters [1], [11], [21], [22], [23]. These studies have generally observed strong seasonal variability of hydrological and biogeochemical properties, but the data are limited to only one year of shipborne measurements [1], [11]. While shipborne measurements provide a high level of granularity, they are relatively limited in both space and time, and it can be difficult to assess general spatial patterns and long-term trends in water quality.

In the absence of a long-term *in situ* dataset, satellite remote-sensing data can be utilized to analyze historical changes in water quality [24], [25], [26]. These approaches are well suited for use in Qatar, as they have been applied to other areas in the Gulf [10], [24], [25], [26], [27], [28], [29], and have been used to monitor optical water quality (OWQ) parameters [e.g.,

Received 18 March 2024; revised 5 August 2024; accepted 31 August 2024. Date of publication 3 September 2024; date of current version 30 September 2024. This work was supported in part by ExxonMobil Research Qatar and NASA Ecological Conservation under Grant 80NSSC20K0076, in part by Ocean Biology and Biogeochemistry under Grant 80NSSC22K1299, and in part by Water Resources Programs under Grant 80NSSC19K1200. *(Corresponding author: Chuanmin Hu.)*

Cheng Xue, Chuanmin Hu, Jennifer P. Cannizzaro, Brian B. Barnes, Jing Shi, and Yuyuan Xie are with the College of Marine Science, University of South Florida, St. Petersburg, FL 33701 USA (e-mail: chengxue@usf.edu; huc@usf.edu; jpatch@usf.edu; bbarnes4@usf.edu; shijing@usf.edu; yuyuan@usf.edu).

Lin Qi is with the NOAA Center for Satellite Applications and Research, College Park, MD 20740 USA, and also with Global Science and Technology, Inc., Greenbelt, MD 20770 USA (e-mail: lin.qi@noaa.gov).

Benjamin D. Jaffe and David A. Palandro are with the ExxonMobil Research Qatar, Qatar Science and Technology Park, Doha 22500, Qatar (e-mail: benjamin.d.jaffe@exxonmobil.com; david.a.palandro@exxonmobil.com).

Digital Object Identifier 10.1109/JSTARS.2024.3454092

chlorophyll-a concentration (Chla; indicator of algal biomass) and SST] [24], [26], [29], [30]. Other important OWQ parameters, such as turbidity (Turb; indicator of suspended sediments), Secchi disk depth (SDD; indicator of water clarity), and floating algae scum (indicator of eutrophication), can also be tracked utilizing remote-sensing data [5], [31], [32], but these variables are notably absent from studies in the Gulf with just a few exceptions [24], [25], [26]. Furthermore, previous studies using satellite remote-sensing data (e.g., Chla) [24], [26], [30] did not consider the possible interference of ocean bottom reflectance in optically shallow waters, which could cause overestimations in OWQ and underestimations in the temporal variability because the bottom is relatively more stable over time than OWQ [33]. Overall, the general OWQ patterns (Chla, water turbidity, water clarity, and floating algae scums) and SST patterns in Qatari coastal waters are largely unknown.

Thus, the objectives of this study are as follows:

1) implement, test, and evaluate the widely utilized remote-sensing algorithms [34], [35], [36], [37], [38], [39], [40], [41] to estimate the water quality variables in Qatari coastal waters;
2) generate water quality time-series maps to assess spatiotemporal patterns;
3) assess long-term water quality trends around Qatar.

The objective #1 is a prerequisite of the other two. Currently, in the absence of a robust and reliable *in situ* dataset, it is not possible to develop and validate locally tuned inversion algorithms specific to Qatari coastal waters. Hence, the widely utilized algorithms are selected based on their principles and performance in other coastal waters [34], [35], [36], [37], [38], [39], [40], [41], which have been extensively validated and accepted by the ocean color research community (hereafter referred to as community-accepted algorithms; see details in Section II) [42], [43], [44], [45]. Then, the spatiotemporal variations of the general water quality are presented. Finally, the uncertainties of the patterns of derived water quality variables are discussed.

II. Data and Method

A. Study Region

Fig. 1(a) shows a true-color image of the Gulf obtained by Moderate-resolution Imaging Spectroradiometer (MODIS)/Aqua on 7 January 2020, and Fig. 1(b) shows the geographic extent (24–27°N, 50–53°E) and bathymetry (data source: GEBCO [46]) of the study region surrounding Qatar. Qatar Peninsula (land mass ∼11 500 km^2) is located along the eastern portion of the Arabian Peninsula and is surrounded by 563 km of coastline, bordering the Gulf to the north and east and the Gulf of Bahrain to the west. Benthic habitats along Qatar's shallow (<20 m) coastal waters include mangrove forests, coral reefs, and seagrass meadows [47], [48], [49].

The climatic features within the region are extreme hot summers, moderate cold winters, high evaporation rates, low precipitation, shamal winds, and dust storms [8]. SSTs often vary over 20 °C between summer and winter. The high evaporation and low precipitation rates result in high salinities, ranging from 40 [4], [22] along the northern and eastern coast up to 70 in the Gulf of Bahrain along the southwestern coast [50]. Deeper waters (>20 m) of the Gulf are characterized by pronounced stratification (thermocline or halocline), while shallow waters are strongly affected by winds that drive water circulation and mixing processes [29]. Winds of various scales and directions dominate the entire Gulf, with the northwesterly (i.e., shamal) winds, northeasterly/easterly (i.e., nashi) winds, and southeasterly/southerly (i.e., kaus) winds having a significant influence on sea surface dynamics [51], [52], [53]. Wind stress and tidal turbulence result in the vertical mixing of the whole water column in shallow nearshore waters and further the sediment resuspension and transport. The stratification of water layers in summer and wind mixings all year long are the primary seasonal factors affecting phytoplankton phenology in the Gulf [26].

TABLE I
Summary of the Four Regions of Interest (ROIs)

ROI	Extent
EEZ	The waters extending from the coast to the outer limit of the Qatar's Exclusive Economic Zone (red line in Fig. 1b).
MTW	Main Territorial Waters, referring to Qatar's Territorial Sea excluding waters around Halul Island (blue line in Fig. 1b).
GoB	Gulf of Bahrain, excluding optically shallow waters (black line in Fig. 1b).
DWR	Deep Water Reference: the waters located offshore in the deep Gulf (green line in Fig. 1b), used as a reference to contrast other ROIs

Four regions of interest (ROIs) were chosen from primarily existing marine boundaries to assess water quality changes [see Fig. 1(b)]. While the ROIs are not mutually exclusive, each area represents potentially different trends related to water depth and distance from shore (see Table I). Two ROIs leverage marine boundaries.[1] Those ROIs are the Main Territorial Waters (MTW) and the Qatar Exclusive Economic Zone (EEZ). The MTW excludes the area surrounding the Halul Island ("*Jazirat Halul*"; located ∼80 km east of Qatar Peninsula) [see Fig. 1(b)]. The third ROI is the Gulf of Bahrain (GoB), which is a semiconstrained water body bordered by Saudia Arabia, Bahrain, and Qatar. The final ROI is the deep-water reference (DWR) and serves as an offshore reference to contrast with the other ROIs.

The productivity of the waters in EEZ is directly linked to eddy circulation in the central Gulf, winter cooling, wind mixing, and disintegration of the cyclonic eddies [22]. Waters in MTW are relatively shallow (<15 m), and the euphotic layer often extends to the sea bottom [29]. The GoB is a nearly enclosed area, and circulation is restricted by coral reefs and the accumulation of sediment. This results in a small tidal range (∼0.5 m) and relatively high salinity (>60), especially in the southern portion (Gulf of Salwah) [50].

[1] [Online]. Available: http://www.marineregions.org/

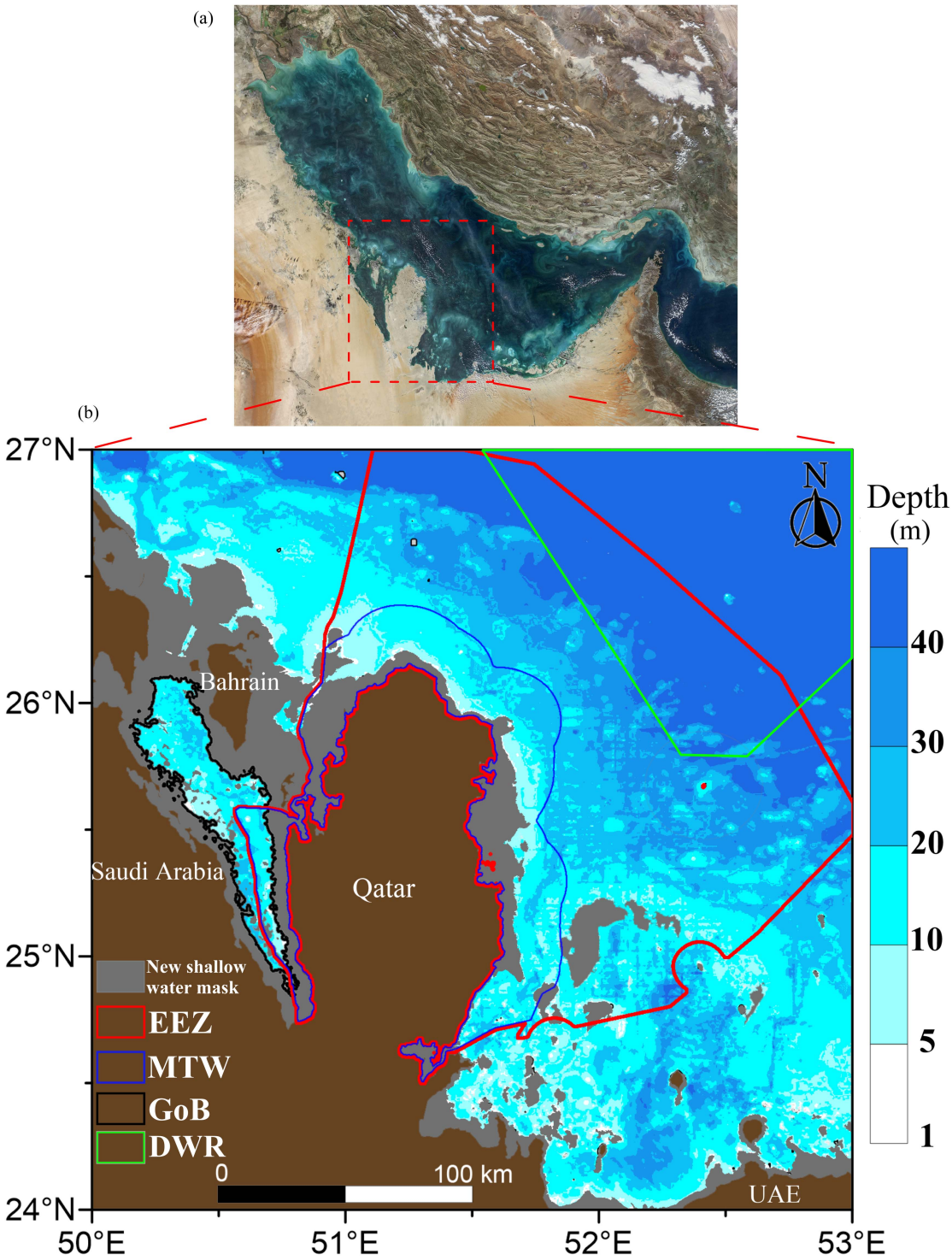

Fig. 1. (a) MODIS/Aqua true-color image of the Gulf collected on 7 January 2020 showing the Gulf, where the study region is outlined by a dashed box. (b) Map of the study region with bathymetry (data source: GEBCO [46]). The four ROIs are EEZ (red), MTW (blue), GoB (black), and DWR (green), respectively (see Table I). Gray represents the optically shallow-water mask developed in Section II-D, and brown represents the land.

B. Water Quality Variables

In this study, the following OWQ variables for near-surface waters surrounding Qatar were examined, with their corresponding algorithms listed in parentheses:

1) chlorophyll-a concentration (Chla in mg m^{-3}) [35], [39];
2) water turbidity (Turb in FNU) [36];
3) water clarity (measured as SDD in m) [37];
4) floating algae density (FD in % cover) [40], [41].

In addition to the above OWQ variables, SST (in °C) was also examined [34], [38].

Due to a lack of consistent field measurements, all data were derived from satellite measurements using established algorithms with a regionally customized shallow-water mask, as shown in Section II-D.

C. Satellite Data Sources

Three types of satellite data were used in this study for different purposes.

First, Sentinel-3 Ocean and Land Color Instrument (OLCI) data were used to define an optically shallow-water mask (see Section II-D). This mask blocks pixels from being used where the shallow bottom interferes with the remotely sensed signal. OLCI data are used because of its higher spatial resolution (300 m) and increased number of spectral bands compared with other medium-resolution sensors.

Second, MODIS data collected aboard Aqua (2002–) were used to estimate the following water quality parameters: Chla, Turb, SDD, and SST. MODIS/Aqua data are suitable for change detection and trend analysis because this dataset provides 20+ years of multiband optical measurements at 1000-m nominal resolution.

Finally, MultiSpectral Instrument (MSI) data collected aboard Sentinel-2A (2015–) and Sentinel-2B (2017–) were used to estimate FD. The two MSI sensors provide a combined five-day revisit frequency at a local time of ∼10:30 A.M. The inclusion of this data was necessary because the surface algae scums are often too small to be detected by OLCI or MODIS, but they are clearly observed in the high-resolution (10–20 m) MSI images [40], [41].

Below we elaborate on the specific data processing steps used for each sensor to meet these individual purposes.

D. Satellite Data Processing

1) OLCI-Based Optically Shallow-Water Mask: Based on the known bathymetry [see Fig. 1(b)] and distribution of shallow benthic features (e.g., coral reefs, seagrass beds, seabed macroalgae, and sand) [47], [48], [49], vast portions of the study area, including water depths < 5 m [33], are optically shallow. Such areas are prone to satellite-retrieved spectral radiance measurements used for deriving water quality parameters that are influenced by reflectance from the bottom [25]. Because of the lack of *in situ* observations of the bottom (depth and type) and water-column optical properties, it is difficult to derive the accurate water quality products from optically shallow water [54]. Therefore, it is essential to apply an optically shallow-water mask to avoid perturbations due to shallow-water bottom.

OLCI/Sentinel-3A (hereafter OLCI/S3A) full-resolution (300 m) Level-1B data for April 2016–December 2022 were downloaded from NASA OB.DAAC[2] and processed to Level-2 data by the OCSSW module (SeaDAS version 8.3, NASA Reprocessing 2022.0) to obtain spectral remote-sensing reflectance (R_{rs}). Then, Level-2 data were reprojected into 250-m Level-3 data, and the multiannual mean data products discussed below were generated. For data quality control, the below 17 flags in l2_flags[3] were used [55]: ATMFAIL, LAND, HIGLINT, HILT, HISATZEN, STRAYLIGHT, CLDICE, COCCOLITH, HISOLZEN, LOWLW, CHLFAIL, NAVWARN, MAXAERITER, CHLWARN, ATMWARN, NAVFAIL, and FILTER.

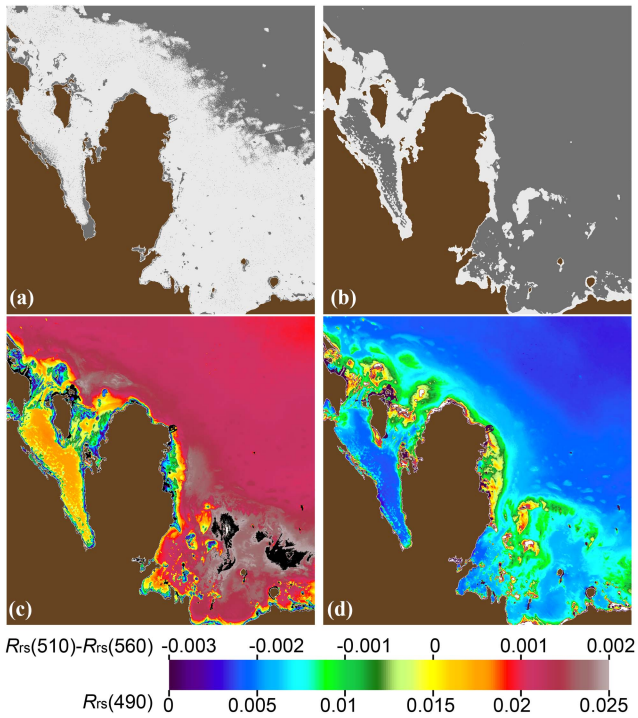

Fig. 2. (a) Typical example of an optically shallow-water mask (light gray region) derived using the default "OPSHAL" l2_flag for OLCI/S3A data on 28 February 2017. (b) New optically shallow-water mask (light gray region) determined in this study. The new mask was determined from OLCI/S3A multiannual mean (c) $R_{rs}(510)$-$R_{rs}(560)$ and (d) $R_{rs}(490)$ using threshold values. All subsequent OWQ analyses excluded the masked pixels. The region with brown color is land.

NASAs satellite ocean color data processing software offers a default Level-2 flag (OPSHAL) for masking optically shallow water, which was developed based on a bathymetry dataset and inherent optical properties retrieved using a quasi-analytical algorithm [33]. OPSHAL was tested but did not work well in the study area because valid pixels were often overmasked and invalid pixels were often undermasked [e.g., Fig. 2(a)]. Thus, this study proposes a new shallow-water mask to exclude optically shallow pixels in Qatari coastal waters.

For Qatari coastal waters, the extent of optically shallow water is difficult to determine because many scattered small subregions deeper than 10 m (for example, areas overlying underwater sand in the GoB) exhibit strong bottom reflectance and the optically active constituents (OACs) of water exhibit strong spatiotemporal variations. Even so, given that the locations of the most optically relevant benthic features are relatively stable

[2][Online]. Available: https://oceancolor.gsfc.nasa.gov

[3][Online]. Available: https://oceancolor.gsfc.nasa.gov/resources/atbd/ocl2flags/

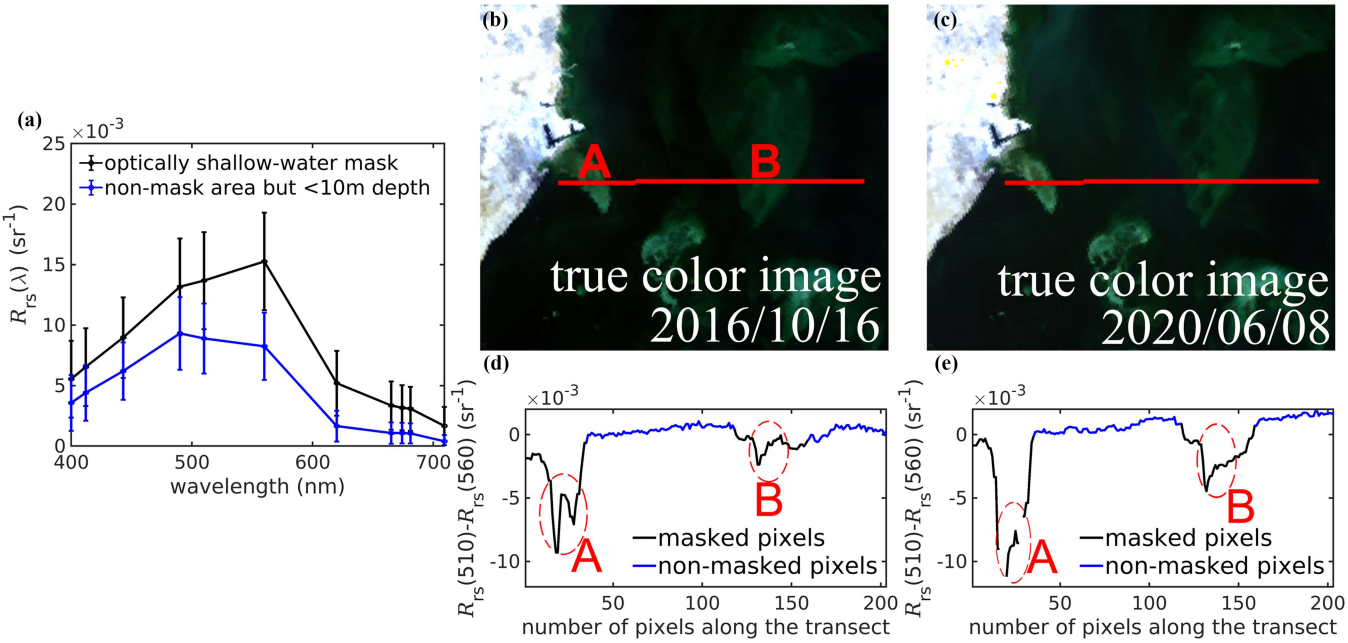

Fig. 3. Demonstration of the effects of optically shallow water on $R_{rs}(\lambda)$ (a) and the validity of the shallow-water mask developed in this study (b)–(e). (a) Mean and standard deviation spectra of $R_{rs}(\lambda)$ from masked pixels and nonmasked pixels. (b) True-color OLCI/S3A image on 16 October 2016 showing bright bottom features (marked as A and B), overlaid with a virtual transect (red line), from which the R_{rs} index is extracted and shown in (d). The masked pixels are annotated in (d). (c) and (e) show another example as in (b) and (d).

over time, an empirical method using OLCI multiannual mean R_{rs} was utilized to determine the extent of optically shallow water. Compared with MODIS, OLCI's higher spatial resolution (300 m) allows it to capture shallow-water bottom features more clearly. Hence, OLCI/S3A data were used to develop the new shallow-water mask, which was downscale sampled for application to MODIS data.

Because optically shallow waters often have $R_{rs}(560) > R_{rs}(510)$ and high $R_{rs}(490)$ values, it was determined that a combination of the variability in OLCI multiannual mean [$R_{rs}(510)$–$R_{rs}(560)$] and $R_{rs}(490)$ can be used to define a static shallow-water mask, as shown in Fig. 2. In these long-term statistics, the negative values in [$R_{rs}(510)$–$R_{rs}(560)$] appear to be associated with bottom sand, coral reefs, and other bottom features for water depths < 5 m. The relatively high values in $R_{rs}(490)$ off the east coast of Qatar appear to be also associated with the bottom where degraded coral reefs are located [47]. So, after multiple trials, the criteria for determining the static shallow-water mask [see Fig. 2(b)] are as follows: [$R_{rs}(510)$–$R_{rs}(560)$] $< -5 \times 10^{-5}$ sr^{-1} for the entire study area, and $R_{rs}(490) > 0.0105$ sr^{-1} for areas off east Qatar only. This mask excludes most areas shallower than 5 m and optically shallow areas in deeper waters with known benthic features [47], [49]. Such a static mask was applied to all images to mask the low-quality pixels before further analysis of temporal trends. Thus, the area-averaged monthly time series of water quality parameters was generated and analyzed for Qatari coastal waters without the effects of optically shallow water.

The contrasts between $R_{rs}(\lambda)$ from masked and nonmasked (but still physically shallow, < 10 m) are shown in Fig. 3(a). It is clear that their spectra are well separated. Fig. 3(b)–(e) further shows the R_{rs} index along an arbitrary transect across both masked and nonmasked pixels. While the true-color images reveal clear shallow-water bottom features, these pixels show dramatic changes in the R_{rs} index, which are successfully masked.

2) MODIS-Based Water Quality: MODIS/Aqua Level-0 data for July 2002–December 2022 were downloaded from NASA OB.DAAC and processed to Level-2 data using the same OCSSW module as used for OLCI/S3A. Level-2 data were then reprojected into 1-km Level-3 data, and the same 17 l2_flags as used for OLCI/S3A were applied. However, because of relatively thick aerosols and frequent sun glint over the Gulf, the thresholds to flag clouds, maximum aerosol optical thickness, and high glint were adjusted from 0.027 to 0.03, 0.3 to 0.5, and 0.005 sr^{-1} to 0.009 sr^{-1}, respectively.

For deriving the OWQ parameters (Chla, Turb, and SDD), community-accepted algorithms were applied to the quality-controlled spectral $R_{rs}(\lambda)$. Of these algorithms, the Chla algorithm is a hybrid between a band difference [35] and band ratio [39] for clear waters and turbid waters, respectively. Because of its empirical nature and usage of blue and green bands, Chla is actually a measure of all water-column OACs, including phytoplankton, colored dissolved organic matter, and suspended nonliving particles. The Turb algorithm was developed for global coastal waters and uses the red (645 nm) and near-infrared (859 nm) bands [36]. It can characterize the suspended particulate matter from low to high concentrations ($\sim$1–200 g m^{-3}). The SDD algorithm [37] utilizes all visible spectral bands and selects the band of maximum light penetration (i.e., minimum light attenuation) to estimate SDD, a measure of water clarity.

For SST, monthly averaged MODIS/Aqua 11 μm daytime and nighttime SST Level-3 data products (4-km resolution, version R2019.0) were downloaded from the NASA OB.DAAC and

analyzed for their spatial variability and long-term trends. In this processing, the quality levels of less than 2 (Level 0 indicates the best quality), which was recorded as qual_sst in the monthly data, were used to exclude low-quality data. SST time series for the entire Gulf and other nearby areas, including the Red Sea and the Northern Arabian Sea, was also obtained in the same way to compare SST trends.

3) MSI-Based Floating Algae Scums: MSI top-of-atmosphere reflectance data from Sentinel-2A (2016–2023) and Sentinel-2B (2017–2023) were downloaded from the Google Earth engine.[4] The spectral bands used here include 490 (B2), 555 (B3), 665 (B4), 740 (B6), and 865 (B8A). Floating algae features were delineated and quantified using a deep learning approach with an overall accuracy of $> 85\%$; such an approach was detailed in [40] and [41] for *Ulva prolifera*, but it was found as effective for the floating algae in the Gulf through visual comparison of the delineated algae scums and the corresponding false-color red–green–blue image following the approach of Qi et al. [56].

After delineation of floating algae features, FD in each pixel was determined using spectral unmixing, where a percent cover (0%–100%) was estimated for each pixel. Then, the original FD images were converted into 4-km grids, which can facilitate visualization of image features in limited space [41]. Annual and monthly composite images and monthly climatology were generated. The monthly FD is regarded as the mean density during the month, and its integration over all grids of each ROI in individual image, after accounting for the grid size, led to the estimate of the total coverage area (m^2) of each ROI during the month.

A total of 18 same-day OLCI images corresponding to the MSI images were used to identify the type of floating algae scums (*Trichodesmium* or green *Noctiluca scintillans*) at the colocated pixels. Compared with MSI, OLCI has more visible spectral bands, including a 620 nm band sensitive to cyanobacteria. The difference of spectral Rayleigh-corrected reflectance [$\Delta R_{\mathrm{rc}}(\lambda)$, dimensionless] between algae scum pixels and nearby water pixels was used for spectral analysis of the algae scums [41], [57].

E. Determine Spatial Pattern and Temporal Variation of Water Quality Parameters

General spatial patterns of OWQ variables (Chla, Turb, and SDD) were evaluated using maps of multiannual means generated from the daily MODIS time series (2002–2022) and corresponding coefficients of variation (CV). CV was calculated as follows:

$$\mathrm{CV} = \mathrm{sd}/M \tag{1}$$

where sd represents the standard deviation and M represents the multiannual mean at each fixed location (pixel). Monthly climatology maps of all water quality parameters were also obtained to examine seasonal patterns.

[4][Online]. Available: https://developers.google.com/earth-engine/datasets/catalog/COPERNICUS_S2_HARMONIZED

The area-averaged monthly mean time series of OWQ parameters (Chla, Turb, and SDD) is obtained to analyze temporal variations of the four subregions. It can be considered that the water quality time series is composed of trend, seasonality, and the residuals components, and so the time-series decomposition method in the statsmodels package of Python [58] is used here with the additive model. The trend can describe gradual changes in long term (over a time scale of >1 year) and, in this decomposition method, it is calculated using (2) where a centered moving average of 12 months was used to assess the trend

$$T_n = \sum_{j=-6}^{6} w_{n+j} M_{n+j} \tag{2}$$

where T_n is the trend component at month n, and M_{n+j} is the monthly observation at month $n+j$. w_{n+j} represents the weight at month $n+j$, which uses weight 1/24 for the first and last month within the window and weight 1/12 for the others. The first and last six observations do not have the corresponding T_n values [58].

Furthermore, the significance (p-value or p) and magnitude (β) of the trend are obtained by the modified Mann–Kendall test [59] and Sen's slope method [60], respectively. These analyses have been widely used to detect long-term water quality change from satellite-derived data across the world [30]. The modified Mann–Kendall test is conducted here with a confidence level of 95% ($\alpha = 0.05$). If $p < \alpha$, then there is a monotonic trend. Sen's slope (i.e., β) is calculated as the median of all the slopes estimated between all the successive data points of a time series as follows:

$$\beta = \mathrm{median}\left[\Delta y/\Delta t\right] \tag{3}$$

where Δy is the change in the time series (y) due to the change in time Δt between two subsequent data. When $p < \alpha$, $\beta > 0$ (or $\beta < 0$) tells that there is an increasing (or decreasing) trend.

For SST, long-term trends for the entire study area, Gulf, Red Sea, and Northern Arabian Sea were determined similar as above. Seasonal SST trends [13] for the entire study region in winter (December–February) and summer (June–August) were also determined.

To observe interannual variability, the monthly time-series data were deseasoned, resulting in monthly anomaly time series. For this purpose, the monthly percentage anomaly (%) was first calculated using (4), and then averaged for three months to observe the temporal anomaly patterns

$$\text{Percentage anomaly} = (\text{monthly} - \text{climatology})/\text{climatology} \times 100\%. \tag{4}$$

III. Results

A. Optical Water Quality

1) General Spatial Distributions: The overall spatial patterns of OWQ variables (Chla, Turb, and SDD) are determined based on the maps of their multiannual means and CVs of these

TABLE II
STATISTICAL SUMMARY OF MULTIANNUAL MEAN CHLA (MG M^{-3}), TURB (FNU), AND SDD (M) OBTAINED FROM DAILY MODIS/AQUA OBSERVATIONS IN 2002–2022 FOR THE FOUR ROIS

	Chla (mg m^{-3})		Turb (FNU)		SDD (m)	
	mean ± std	min–max	mean ± std	min–max	mean ± std	min–max
EEZ	1.21±0.22	0.91–3.14	0.59±0.37	0.19–2.90	9.71±1.42	3.06–11.61
MTW	1.56±0.36	1.12–3.14	1.10±0.42	0.25–2.90	7.49±1.10	3.06–9.85
GoB	2.27±0.26	1.92–3.14	0.43±0.10	0.31–0.97	7.42±0.31	6.18–7.95
DWR	1.16±0.11	0.96–1.66	0.28±0.03	0.23–0.43	11.13±0.30	9.57–11.74

Note: The std means the standard deviation.

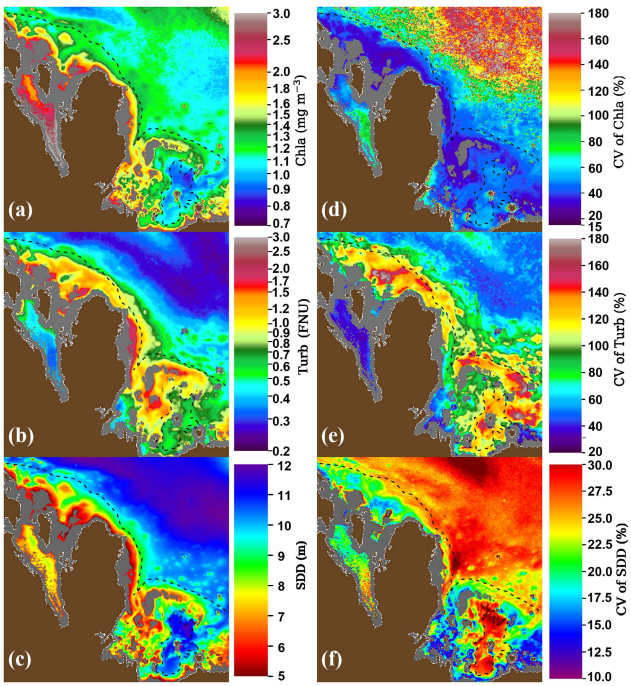

Fig. 4. General spatial distributions of water quality parameters obtained from MODIS/Aqua observations in 2002–2022. (a)–(c) are the multiannual means of Chla (mg m^{-3}), Turb (FNU), and SDD (m), respectively, and (d)–(f) are the corresponding CV (%) of Chla, Turb, and SDD, respectively. The black dash line represents the water depth of ∼ 20 m. The gray region shows the OLCI-based optically shallow-water mask. The region with brown color is land.

mean values obtained from daily MODIS/Aqua observations in 2002–2022 (see Fig. 4). Statistical summaries of these values for the four ROIs are provided in Tables II and III.

Multiannual mean Chla, Turb, and SDD exhibit strong spatial variability from nearshore to offshore waters. Chla mostly decreases and SDD increases with distance offshore. Turb exhibits a similar spatial pattern as Chla, except for in the GoB where Turb is relatively low (∼ 0.3–0.4 FNU) with values similar to those observed in deeper, offshore waters (∼ 0.2 FNU). In general, water quality spatial patterns in the study area can be intuitively divided into three regions starting from the southwest to the northeast, in order: the GoB with high Chla, low Turb, and moderate SDD; the shallow nearshore zone (water depths < 20 m) along Bahrain Island and Qatar Peninsula with high Chla and Turb and low SDD, as well as the strong spatial gradients; and the deep-water offshore zone (water depths > 20 m) with low Chla, low Turb, and high SDD.

Multiannual mean Chla throughout the entire study area ranges from ∼0.6 to ∼3 mg m^{-3} and CVs of Chla exhibit high variability (26.5%–311.1%) [see Fig. 4(a) and (d)]. The highest mean Chla (2.27 mg m^{-3}) was observed in the GoB where values > 3 mg m^{-3} frequently occurred in the Gulf of Salwah. Mean Chla was also relatively high (1.56 mg m^{-3}) in the MTW zone where sharp spatial gradients were observed. The mean CV of Chla in both of these regions was relatively low (< 60%), indicating minimal change over time. In contrast, the EEZ and DWR zones exhibited lower mean Chla (∼1.2 mg m^{-3}) and relatively high mean CV of Chla (>80%). The higher CVs in these regions mainly occur in deeper waters and are a result of intermittent algal bloom events [28]. This indicates that Chla plays a large role in driving water quality in offshore waters.

Multiannual mean Turb in the study area ranges from ∼0.2 to ∼3.0 FNU and similar to Chla CVs of Turb also exhibit high variability (5.8%–170.5%) [see Fig. 4(b) and (e)]. Mean Turb and mean CV of Turb are relatively high in the MTW (1.10 FNU and 101.1%, respectively) and EEZ (0.59 FNU and 82.6%, respectively) compared with the GoB (0.43 FNU and 37.9%, respectively) and DWR (0.28 FNU and 52.3%, respectively). A large belt of high mean Turb (>1 FNU) is evident in nearshore waters north and east of Qatar Peninsula [see Fig. 4(b)]. This area (7650 km^2) also exhibits high CV of Turb (>120%), which indicates that water quality in the shallow nearshore zone is mainly controlled by sediment resuspension events.

Multiannual mean SDD in the study area ranges from ∼5 to ∼12 m, but unlike Chla and Turb, CV of SDD exhibits relatively low variability (2.2%–40.8%) [see Fig. 4(c) and (f)]. Mean SDD increases steadily from regions that primarily consist of nearshore waters, including the GoB (7.42 m) and MTW (7.49 m), to regions with deeper waters, including the EEZ (9.71 m) and the DWR (11.13 m). SDD spatial patterns reflect the features of Chla and Turb combined.

2) Monthly Climatology and Seasonal Variability: The CVs of multiannual mean Chla, Turb, and SDD, as shown in Fig. 4, highlight the overall variability observed over the past 20 years. In this section, OWQ variability is examined on an intra-annual

TABLE III
STATISTICAL SUMMARY OF THE CV (%) OF MULTIANNUAL MEAN CHLA, TURB, AND SDD OBTAINED FROM DAILY MODIS/AQUA OBSERVATIONS IN 2002–2022 FOR THE FOUR ROIS

	CV of Chla (%)		CV of Turb (%)		CV of SDD (%)	
	mean ± std	min−max	mean ± std	min−max	mean ± std	min−max
EEZ	81.0±45.2	26.5−291.0	82.6±29.4	5.8−170.5	25.0±2.7	2.2−40.3
MTW	41.9±14.4	27.1−189.3	101.1±29.0	5.8−151.4	22.4±3.7	2.2−32.2
GoB	59.3±14.9	33.7−98.5	37.9± 2.7	28.5−47.9	20.9±2.0	16.4−28.2
DWR	143.9±28.9	52.3−311.1	52.3± 7.3	39.6−96.4	27.2±1.5	23.2−40.8

Note: The std means the standard deviation.

scale using monthly climatology maps (see Fig. 5). Fig. 6 shows the seasonality of each OWQ variable for the individual ROIs.

For the DWR, strong seasonal variability was observed for Chla and SDD. Minimal Chla ($\sim$ 0.6 mg m^{-3}) and maximal SDD ($\sim$ 15 m) occur in late spring and summer. In winter, Chla often exceeds $\sim$ 2 mg m^{-3} and SDD is generally less than $\sim$ 10 m. Elevated wintertime Chla is consistent with observations of toxic dinoflagellate blooms in Gulf waters [28]. Compared with Chla and SDD, Turb in the DWR shows weak seasonal variability with relatively low monthly values ranging from $\sim$0.2 to 0.3 FNU.

Similar to the DWR, the GoB exhibits relatively low Turb ($\sim$0.4–0.6 FNU) that changes minimally throughout the year. Chla and SDD also display low seasonal variability in this region with maximal Chla ($\sim$ 3.5 mg m^{-3}) and minimal SDD ($\sim$ 6 m) in the fall and minimal Chla ($\sim$ 1.5 mg m^{-3}) and maximal SDD ($\sim$ 8 m) in early spring. Spatially, the southern GoB (or Gulf of Salwah) generally exhibits higher Chla ($>$ 2 mg m^{-3}) and lower Turb ($\sim$0.3 FNU) compared with northern GoB waters [see Fig. 5(a) and (b)]. This pattern was generally observed year round.

Seasonal patterns of OWQ variability in the EEZ and MTW zones were also often observed. Both regions exhibited strong seasonal variability in Turb with lower values observed in late spring and summer compared with winter. Turb values ranged from $\sim$0.4 to 0.8 FNU in the EEZ and $\sim$0.7 to 1.4 FNU in the MTW zone. Moderate seasonal variability for Chla and SSD was observed in the EEZ with similar patterns as the DWR. Weak seasonal variability for Chla and SDD was observed in the MTW with patterns similar to the GoB.

3) Long-Term Changes: The time series showing changes in monthly mean OWQ (Chla, Turb, and SDD) for the four ROIs is shown in Fig. 7. This provides an overall picture of the complexity of OWQ variations in Qatari coastal waters. High fluctuations in OWQ were observed throughout the entire study period (2002–2022) that were dominated by the seasonal component. After removing seasonality, the anomaly time series (see Fig. 8) still shows obvious water quality fluctuations in many months. The positive Chla anomaly values from the DWR indicate algal bloom events, such as the dinoflagellate bloom during 2008 and 2009. SDD anomalies from the DWR are highly correlated with Chla anomalies ($R = 0.86$ and $p < 0.001$), suggesting that the SDD anomalies are also caused by the algal bloom events. In addition, Chla anomalies between the EEZ and MTW zones show a strong correlation ($R = 0.69$ and $p < 0.001$), suggesting that the temporal changes of Chla in the EEZ were dominated by those of the DWR, followed by those of the MTW.

TABLE IV
p-VALUE (p) AND MAGNITUDE (β) OF LONG-TERM TREND COMPONENTS OF CHLA, TURB, AND SDD IN THE ROIS OBTAINED FROM MODIS/AQUA OBSERVATIONS IN 2002 AND 2022

	$Chla_t$		$Turb_t$		SDD_t	
	p	β	p	β	p	β
EEZ	0.00	−0.12	0.00	−0.029	0.00	0.39
MTW	0.00	−0.13	0.00	−0.053	0.00	0.28
GoB	0.03	0.08	0.01	−0.029	0.27	0.03
DWR	0.00	−0.08	0.00	−0.013	0.00	0.37

Note: β of Chla, Turb, and SDD are in mg m^{-3} decade^{-1}, FNU decade^{-1}, and m decade^{-1}, respectively.

Long-term changes are difficult to determine based on these monthly time series because of perturbations caused by seasonal variability and interannual fluctuations. Therefore, trend components are obtained using the monthly time series to indicate their long-term changes over 20 years.

Fig. 9 shows the long-term trend components of Chla, Turb, and SDD (denoted as $Chla_t$, $Turb_t$, and SDD_t, respectively) for the four ROIs, and the magnitude and significance of these trends are recorded in Table IV. Long-term trends for all OWQ variables are statistically significant in the EEZ, MTW, and DWR zones. For the GoB, $Chla_t$ and $Turb_t$ show statistically significant trends, while SDD_t ($p = 0.27$) does not. Chla shows an increasing trend (0.08 mg m^{-3} decade^{-1}) in the GoB, but decreasing trend in the other three ROIs. The fastest decrease in Chla was observed for the MTW (−0.13 mg m^{-3} decade^{-1}), followed by the EEZ (−0.12 mg m^{-3} decade^{-1}), and DWR (−0.08 mg m^{-3} decade^{-1}). All ROIs showed decreasing Turb with the greatest change observed in the MTW (−0.053 FNU decade^{-1}), followed by the EEZ and GoB (−0.029 FNU decade^{-1}), and the DWR (−0.013 FNU decade^{-1}). SDD shows increasing trends in the EEZ (0.39 m decade^{-1}), DWR (0.37 m decade^{-1}), and MTW (0.28 m decade^{-1}). Overall, these results indicate that Chla and Turb are mostly decreasing in Qatari

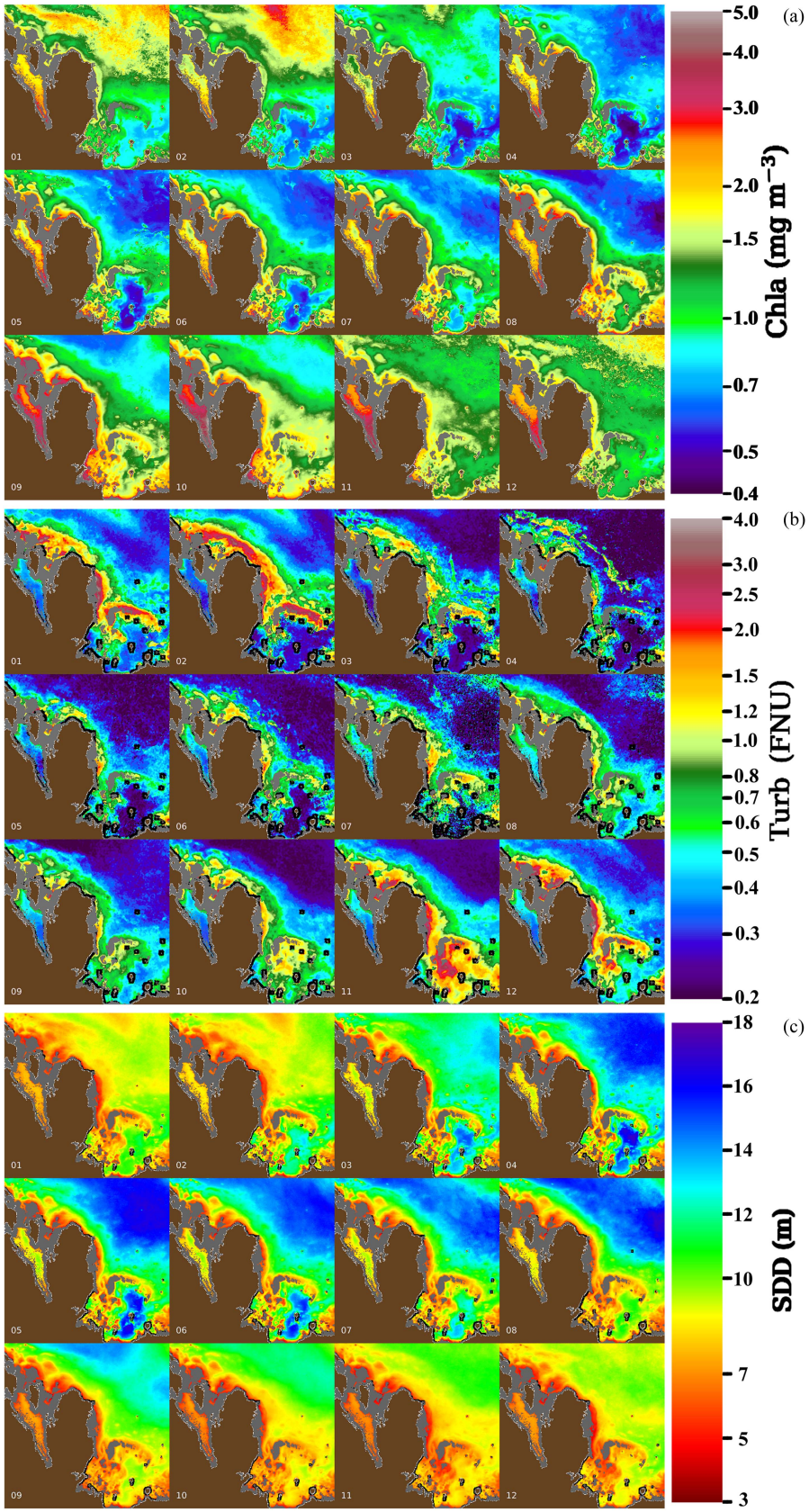

Fig. 5. Monthly climatology maps of (a) Chla (mg m^{-3}), (b) Turb (FNU), and (c) SDD (m) obtained from MODIS/Aqua observations in 2002 and 2022. The gray region shows the OLCI-based optically shallow-water mask. The region with brown color is land. The black areas represent regions with no valid data.

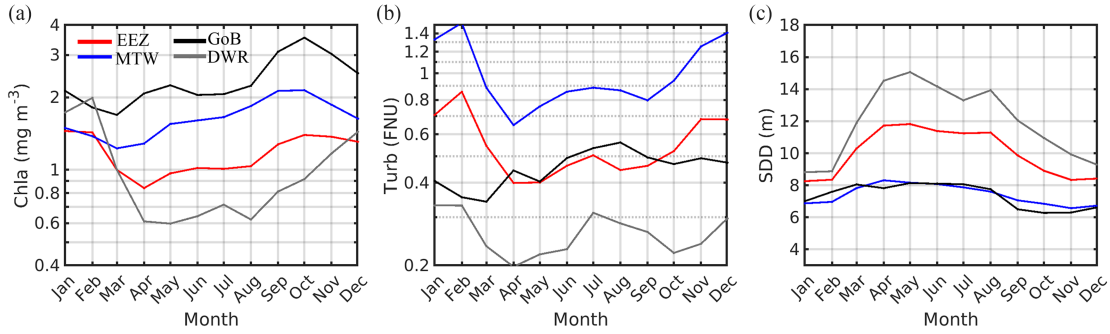

Fig. 6. Monthly climatological means of (a) Chla (mg m^{-3}), (b) Turb (FNU), and (c) SDD (m) in the ROIs obtained from MODIS/Aqua observations in 2002 and 2022. The EEZ, MTW, GoB, and DWR zones are represented by the red, blue, black, and gray lines, respectively.

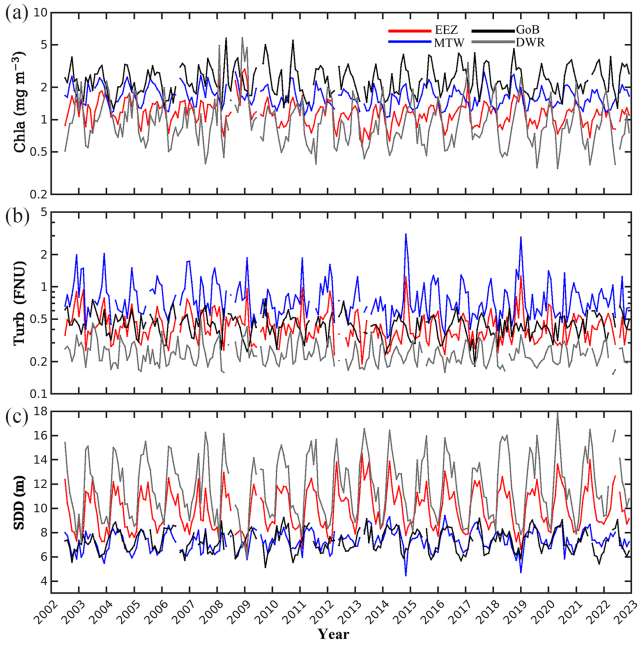

Fig. 7. Monthly mean time series of (a) Chla (mg m^{-3}), (b) Turb (FNU), and (c) SDD (m) in the ROIs obtained from MODIS/Aqua observations in 2002 and 2022. The EEZ, MTW, GoB, and DWR zones are represented by the red, blue, black, and gray lines, respectively.

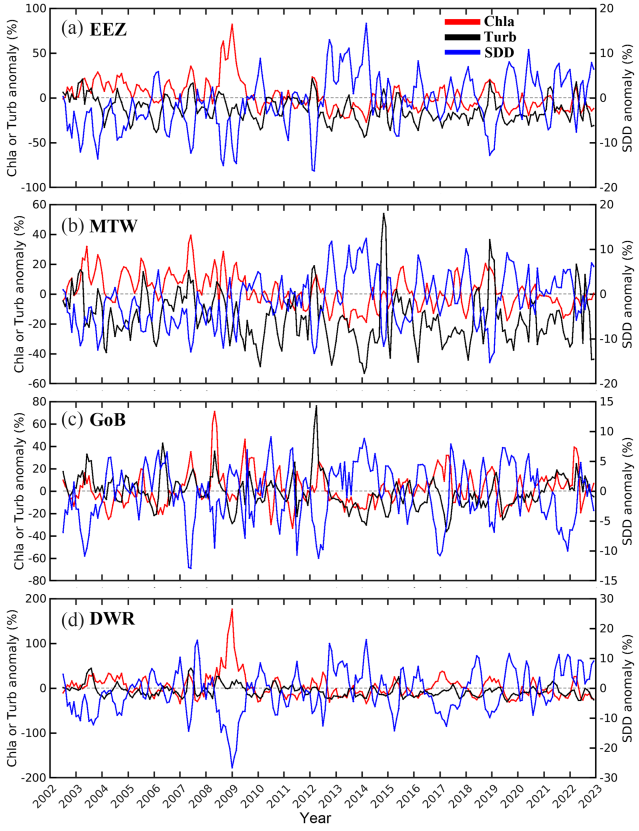

Fig. 8. MODIS/Aqua time series of the percentage anomaly of Chla (red lines), Turb (black lines), and SDD (blue lines) in (a) EEZ, (b) MTW, (c) GoB, and (d) DWR between 2002 and 2022.

coastal waters (with the exception being the GoB), and as a result, SDD (i.e., water clarity) is increasing. However, these rates of change are relatively small when compared with the multiannual means (see Table II).

B. Sea Surface Temperature

SST exhibits strong seasonal variability in Qatari coastal waters with temperatures as high as $\sim 38\,^{\circ}C$ in summer and as low as $\sim 17\,^{\circ}C$ in winter [see Fig. 10(a)]. Because minimal variability was observed between the four ROIs [see Fig. 10(b)], long-term trends in SST for the entire study area [see Fig. 1(b)] were examined and compared with neighboring areas. Statistically significant ($p < 0.05$) warming trends were observed for all regions (this study area, Gulf, Red Sea, and Northern Arabian Sea) and seasons (winter and summer for this study area only) that were examined.

SST_t shows significant warming trends in the study area during both daytime (0.64 °C/decade) and nighttime (0.64 °C/decade) [see Fig. 11(a)]. These trends were slightly higher in the winter (December–February) (0.89–0.92 °C/decade) compared with the summer (June–August) (0.56–0.73 °C/decade) [see Fig. 11(b) and (c)] and were similar to trends observed for the entire Gulf (0.62–0.64 °C/decade) [see Fig. 11(d)]. Qatari coastal waters are warming ~2–3 times faster

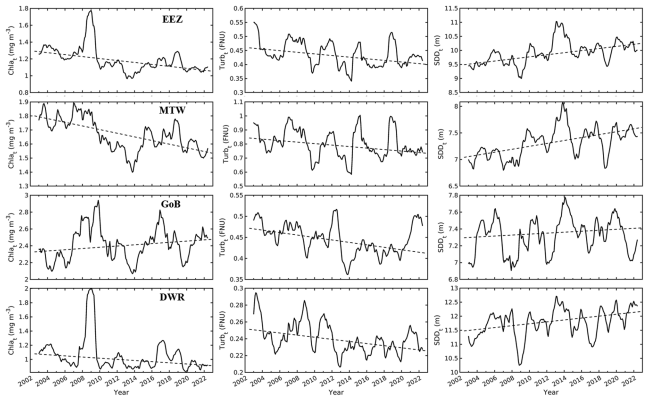

Fig. 9. Long-term trend components of Chla (mg m^{-3}) (left column), Turb (FNU) (middle column), and SDD (m) (right column) in the ROIs obtained from MODIS/Aqua observations in 2002 and 2022. The panels from the top to the bottom correspond to the following ROIs: EEZ, MTW, GoB, and DWR zones. The dashed lines are linear trend-fitting lines. A statistical summary of these relationships is provided in Table IV.

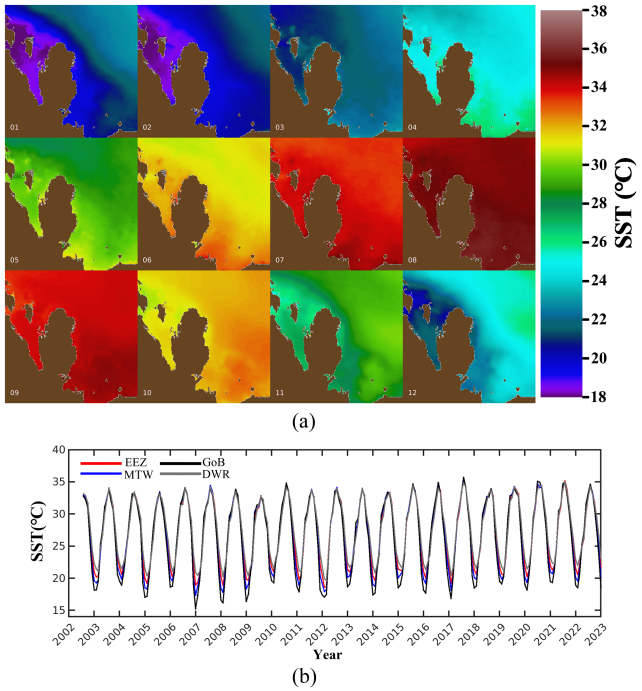

Fig. 10. (a) Monthly climatology maps of daytime SST (°C) obtained from MODIS/Aqua in 2002–2022. The region with brown color is land. (b) Monthly mean daytime SST (°C) for the ROIs obtained from MODIS/Aqua observations in 2002–2022. The EEZ, MTW, GoB, and DWR zones are represented by the red, blue, black, and gray lines, respectively.

than the Red Sea and Northern Arabian Sea [see Fig. 11(e) and (f)] and ∼8 times faster than the global oceans [13].

C. Floating Algae

Annual and monthly mean climatology maps of floating algae density are shown in Fig. 12, and the temporal variations of algae scum coverage in the ROIs in 2016–2023 are shown in Fig. 13.

Fig. 12(a) and (b) shows the annual mean and monthly mean climatology images of MSI FD between 2016 and 2023, respectively. Unlike for the OWQ parameters (Chla, Turb, and SDD), FD did not show gradual spatiotemporal variations. The algae scums occurred at various densities and extents with time, from the shallow nearshore to the offshore. Usually, small-scale algae scums slicks showed low density and low coverage around Qatari coastal waters, particularly during August–November. However, some intensive algae scums did occur in EEZ. For example, extensive algae scums with high FD were observed off the northeast of Qatar in 2016 (April) and off the north of Qatar in 2017 (June) (see Fig. 12). Such intensive algae scums did not show up again in the EEZ from 2018 to 2023, indicating high interannual variability.

Fig. 13 shows that EEZ has the maximum climatology coverage of algae scums in June ($\sim 1.7 \times 10^6$ m^2) because of the intensive algae scums in June 2017 (coverage $\sim 2.4 \times 10^6$ m^2). In the same month, MTW also has its own maximum monthly and climatological coverage up to $\sim 2.0 \times 10^5$ m^2 that is an order of magnitude lower than that of EEZ. Thus, the area with higher FD and larger extent of algae scums ranged from the nearshore waters in the MTW toward the deep waters within the EEZ boundary in June 2017. In April 2016, DWR showed the maximum values of monthly ($\sim 2.3 \times 10^6$ m^2) and climatological coverage ($\sim 1.4 \times 10^6$ m^2), which is at the same order as the maximum coverage of EEZ. And EEZ has the second peak climatology coverage up to $\sim 1.1 \times 10^6$ m^2 in April because of the high coverage in April 2016. Except for April and June, EEZ shows the climatology coverage of more than 1.0×10^5 m^2 in March, May, July, and September, while DWR shows that in May, September, and the winter months. The relatively high climatology coverage in MTW ($> 1 \times 10^5$ m^2) and GoB ($> 1 \times 10^4$ m^2) showed in June and the summer months, respectively. Fig. 12 indicates that the coverage difference of algae scums is attributed to the spatial pattern of high FD rather than the extent size of ROI. Thus, in summary, high FD of algae scums often occurred in the offshore. Moreover, large extents of algae scums often occurred in EEZ during the spring and summer months, and in DWR during the winter and summer months.

A total of 18 matching images between OLCI and MSI were found with algae scums in December–June, August, and October during 2016–2022, and algae scums of high FD could be observed in 7 of them. The algae scums appear greenish in the FRGB images. $\Delta R_{rc}(\lambda)$ in summer months exhibits local reflectance maximum around 620 nm, with a slight decrease at 560 nm. These are characteristics of *Trichodesmium* [57], and these features were also observed in the other matching images during spring to autumn. For winter months, $\Delta R_{rc}(\lambda)$ shows the reflectance approaching zero at blue bands and the local reflectance maximum around 560 nm, which were consistent with the spectral features in the other matching images in winter, and it can be inferred as green *Noctiluca scintillans*. Thus, the algae scums type occurred in winter months is identified as green *Noctiluca scintillans*, while that occurred from spring to autumn is identified as *Trichodesmium*, which agrees with the reported field observations and phytoplankton enumeration data elsewhere in the Gulf [21], [61], [62], [63].

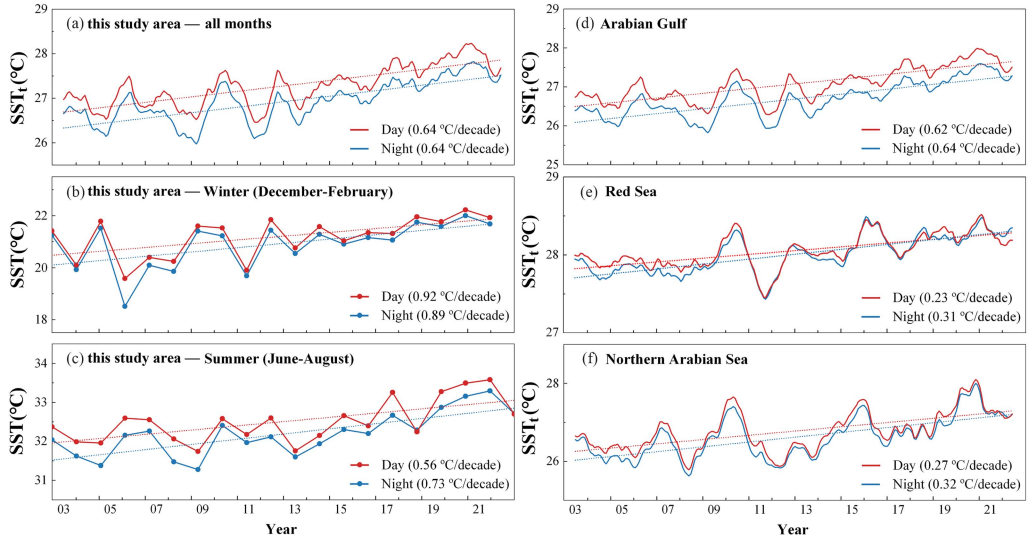

Fig. 11. Long-term trend components of daytime (red lines) and nighttime (blue lines) SST (°C) obtained from MODIS/Aqua observations in 2002–2022 for (a) this study area, (d) entire Gulf, (e) Red Sea, and (f) Northern Arabian Sea. Similarly, seasonal SST trends for this study area were determined for (b) winter and (c) summer only. The dotted lines are linear trend-fitting lines, and their slopes (β) corresponding to the warming rates are included.

IV. Discussion

A. Main Findings

This study examined spatial/seasonal patterns and long-term trends of OWQ and water temperature in Qatari coastal waters using $>$ 20 years of satellite ocean color data and SST data. It supplements and expands upon the previous efforts focused mainly on investigating changes in satellite-derived Chla and SST in this region [10], [25], [26], [28], [29].

Here, optically shallow waters that are known to impact retrieval accuracies are excluded and additional water quality parameters (Turb, SDD, and floating algae) are examined.

OWQ in Qatari coastal waters showed high spatial variability with strong nearshore–offshore gradients. Generally, Chla and Turb were higher and SDD was lower in shallow, nearshore waters ($<$ 20 m) compared with deeper offshore waters. Such values were relatively low compared with other turbid coastal regions, especially those heavily impacted by estuarine outflow [31], [36]. As a result, vast areas surrounding Qatar Peninsula, where light effectively reaches the bottom, are optically shallow and, therefore, require masking to prevent overestimations in Chla/Turb and underestimations in SDD [see Fig. 2(b)] [29].

Water clarity in the MTW and EEZ zones is mainly controlled by changes in resuspended sediments and algal blooms, respectively. Algal blooms observed in deep offshore waters may be used as a warning for bloom transport to nearshore waters [10], [28], [29] given the strong correlation observed between monthly Chla anomalies in the EEZ and DWR. High spatial, seasonal, and interannual variability was observed for floating algal scums. Based on the spectral shapes of the algal scums, these events were found to be mainly caused by green *Noctiluca scintillans* in winter months and *Trichodesmium* in spring and summer months.

Strong seasonal variability in OWQ was also observed. The seasonality of Chla and SST found in this study is consistent with that reported previously for the entire Gulf [26], [30]. Long-term Chla trends (-0.12 mg m^{-3} decade^{-1}) were mostly consistent with previous studies for the EEZ [30], [64]. Moradi [30] found slightly higher decreasing Chla trends (-0.14 to -0.23 mg m^{-3} decade^{-1}) for the Gulf in 2002–2018. However, overall, these rates of changes while statistically significant are relatively low compared with multiannual means (see Fig. 4), indicating minimal change.

Qatari coastal waters are warming at a rate ($\sim$0.6 °C/decade) similar to the entire Gulf, but $\sim$2–3 times faster than surrounding areas (Red Sea and Northern Arabian Sea) and $\sim$8 times faster than the global oceans [13]. The warming rate determined for the entire Gulf agrees with previous studies [30], [64]. Increased temperature may impact marine biodiversity and associated fisheries in Gulf waters [65]. More specifically, bottom hypoxia, HABs, and coral bleaching events have all been linked to warming waters [3], [8], [66], [67].

B. Uncertainties

While SST and FD derived from satellite measurements have been shown to be reliable even for optically shallow waters and optically complex turbid waters [41], [68], interpretations of OWQ data derived from satellite measurements over optically complex waters require caution, especially when there is lack of *in situ* data to validate the observed spatial and temporal patterns. Nevertheless, the OWQ data were estimated using the community-accepted algorithms, and in the future, they can be improved once large quantity of *in situ* data is available to fine-tune the algorithms or develop new algorithms. The uncertainties in the estimated OWQ originate from both optical complexity of water [25] and atmospheric correction errors in the blue bands [69]. However, based on the published literature, such uncertainties should have minimal impacts on the derived spatial patterns and temporal changes of the OWQ. This is especially

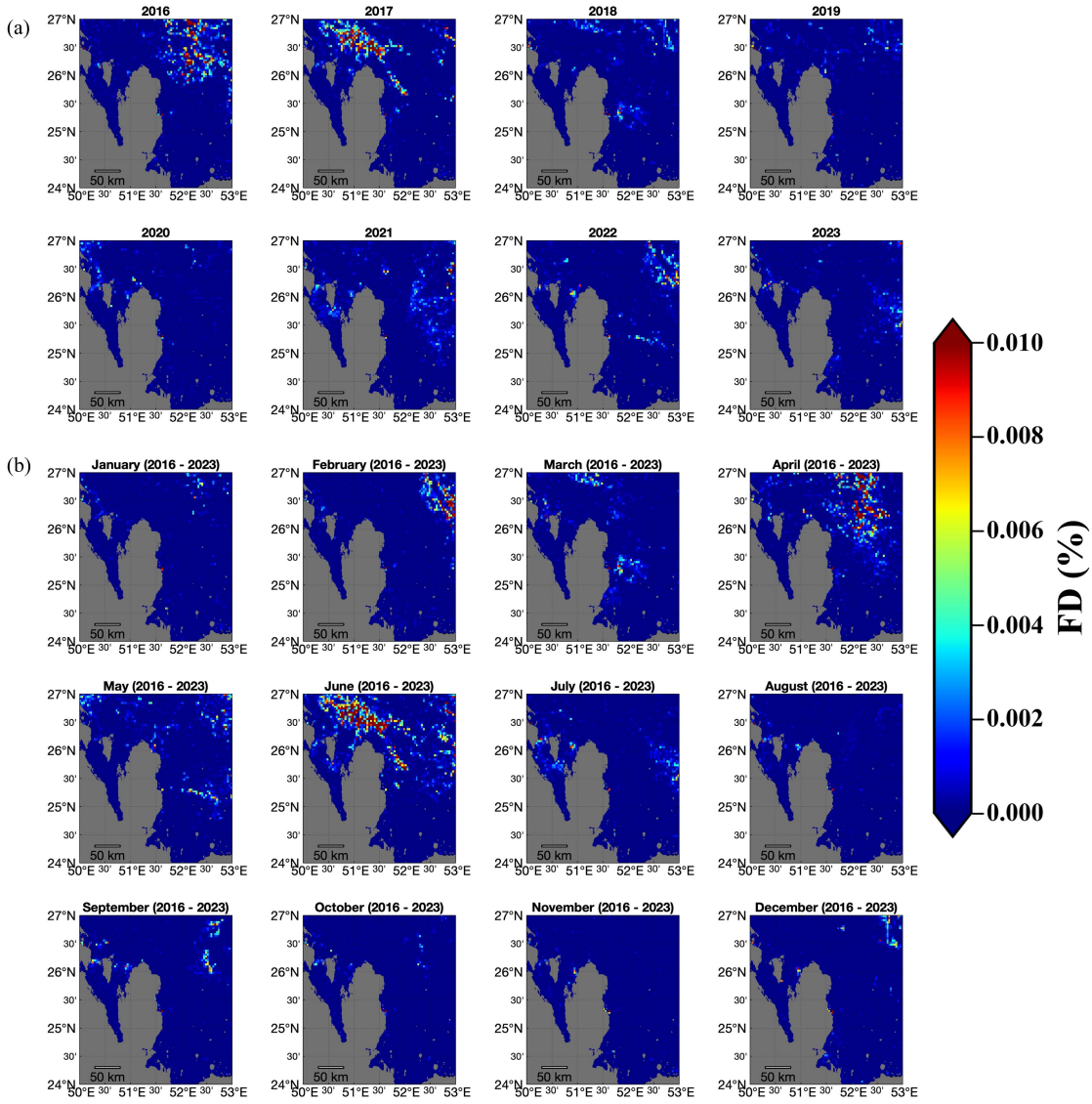

Fig. 12. (a) Annual and (b) monthly climatology maps of FD (%) obtained from MSI/Sentinel-2 observations in 2016–2023. The region with gray color is land.

true for SDD and Turb as they were derived from spectral bands of > 490 nm. Chla, on the other hand, is different because the blue band used in the algorithm can be affected significantly by OACs other than phytoplankton.

For this reason, Chla uncertainties can vary substantially across different water types. For deep waters in this study, Chla is believed to be reliable because optical properties appear to be dominated by algal particles without interference of the shallow bottom [11]. The positive anomalies in 2008 and 2009 correspond to the reported blooms [10], with a strong correlation ($R = 0.82$) between the EEZ and DWR, suggesting the usefulness of Chla as an index of concentration of algal particles. Such an argument appears reasonable even for the turbid coastal waters within the MTW ROI, where Chla variations are consistent with those reported from field observations [11] and reasonable agreement was found between satellite-derived Chla and field-measured Chla ($R \sim 0.8$, [70]). Specifically, Chla decreases from summer to winter with larger spatial variability in winter but higher Chla in summer in nearshore waters [see Figs. 5(a) and 6]. This is possibly because of the small interference of nonalgal articles [Turb $< \sim 4$ FNU, Fig. 5(b)].

The GoB, however, appears to be a special case that requires extra caution. The water is relatively clear (Turb < 0.6 FNU) throughout the year, yet Chla is even higher (>1.5 mg m^{-3}) than in bloom waters of the DWR. Such a disparity is despite the high-quality assurance score (0.8–0.9) of the MODIS $R_{rs}(\lambda)$ [71] in the presence of possible dust particles [72], [73]. Thus, the reasons behind the high Chla in the GoB despite the low turbidity need to be explored further, especially through targeted field measurements of Chla and turbidity as well as $R_{rs}(\lambda)$ and other optical properties, such as absorption and scattering coefficients.

Due to technical difficulties, optically shallow waters were masked in this study [see Fig. 2(b)]. These are within the MTW zone that could be affected by land-based discharges, especially under increased human activities. Although it is suspected that they are in phase with adjacent, optically deep waters, future

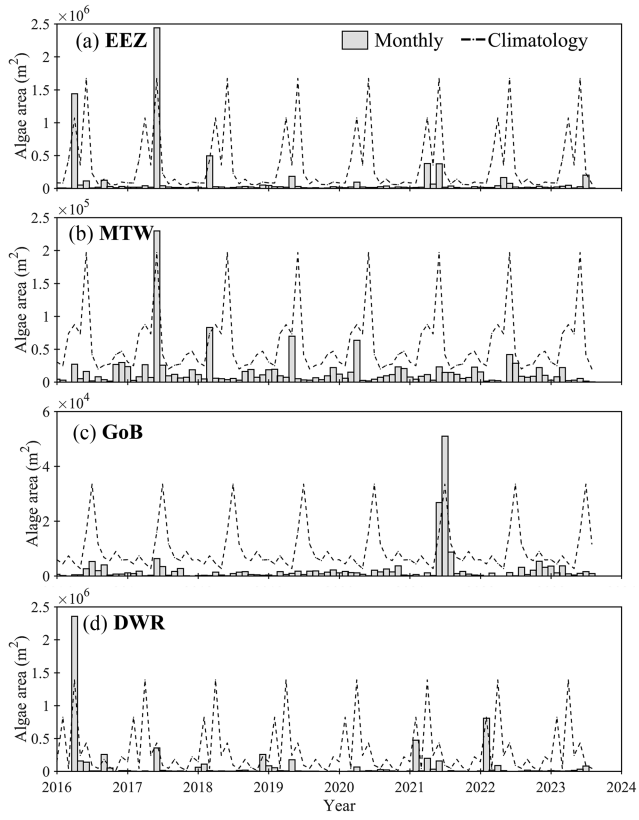

Fig. 13. Monthly floating algae areal coverage (m^2) in the (a) EEZ, (b) MTW, and (c) GoB, and (d) DWR zones obtained from MSI/Sentinel-2 observations in 2016–2023. The monthly climatological coverage (dashed lines) is overlaid. The panels from the top to the bottom correspond to the ROIs EEZ, MTW, GoB, and DWR, respectively.

studies should focus on these waters since studies on briny discharge suggest very localized impacts [18], [19].

C. Future Perspectives

There is a clear need to develop local algorithms, especially for optically shallow waters. To meet such a need and based on the observed strong seasonality, it is suggested that these waters are sampled at least once per season to cover the dynamic range and different environmental conditions. In addition to field measurements to improve algorithms and validate the observed patterns, more satellites are required to assure continuity, especially when considering that 1) MODIS will stop functioning by 2026 and 2) it often takes several decades to observe long-term trends. Such multisensor long-term observations require cross-sensor consistency. While there are many ocean color sensors currently in orbit, the example in Fig. 14 shows that consistent observations can be obtained from the OLCI/S3A measurements.

The scatter and histogram comparisons of Chla obtained from MODIS/Aqua and OLCI/S3A for the entire study area in 2016–2022 are shown in Fig. 14(a) and (c). Despite the slightly higher MODIS-derived Chla for midrange values, Chla obtained from MODIS and OLCI agrees with each other in most pixels and their correlation coefficient is 0.7. The difference of Chla between

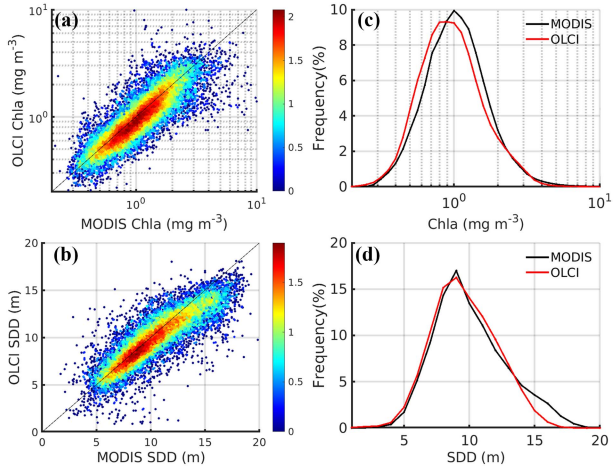

Fig. 14. Comparisons of monthly mean Chla and SDD obtained from MODIS/Aqua and OLCI/S3A observations in the entire study area in 2016–2022. (a) and (b) are scatter plots of Chla and SDD, and (c) and (d) are their histograms, respectively. In the scatter plots, the black solid line represents the 1:1 line, and the color represents the density of the points on a $\log_{10}$ scale.

MODIS and OLCI could be caused by the combined effects of the different bands used in the inversion algorithms [39] and the different spatial resolutions. As a reference, SDD is also compared and Fig. 14(b) and (d) shows the comparisons. Because the SDD algorithm [37] uses all visible bands weakening the effect of different band sets, the correlation coefficient of SDD is higher (0.87) and the histograms compare closely, especially for SDD $<$ 15 m. Although there is still the difference of spatial resolution, the agreement between MODIS and OLCI may improve further if *in situ* dataset can be used for recalibrating and validating the algorithms.

V. Conclusion

Due to limited resources, *in situ* data are often limited or nonexistent in many regions around the globe despite the importance of understanding water quality patterns. In the absence of such *in situ* data, this case study uses Qatari coastal waters as an example to demonstrate how spatiotemporal variations of the general water quality can be obtained from satellite remote sensing, which can provide Optical Water Quality (OWQ) and SST data. This is through the use of the community-accepted algorithms that have been implemented, tested, and evaluated for Qatari waters [70], [71], together with considerations to exclude low-quality data through the use of l2_flags [55] and a customized optically shallow-water mask.

Such an effort led to the knowledge of spatial distribution patterns and temporal changes of several water quality parameters for the period of 2002–2022. In general, strong seasonality was found in all water quality parameters (Chla, Turb, SDD, SST, and FD) in this study. While most of them showed no dramatic long-term changes, SST showed a higher warming rate than the adjacent Red Sea and Arabian Sea. Whether such trends will sustain in the future requires continuous assessment using consistent satellite data and algorithms.

In future studies, the method of estimating water quality parameters in optically shallow waters should be developed, and more field observations should be conducted in nearshore waters to account for the large gradients. In addition, the use of high-resolution sensors is necessary to monitor algae scums as a proxy of HABs. Finally, Qatari coastal waters are not isolated but connected to other Gulf waters, thus requiring international collaborations to measure and understand water quality patterns and trends across the maritime boundaries [8].

ACKNOWLEDGMENT

The authors would like to thank the NASA Ocean Biology Distributed Active Archive Center (OB.DAAC) for the satellite data and the NASA Ocean Biology Processing Group for providing the software tools, and the two anonymous reviewers for their help to improve the presentation of this work. The scientific results and conclusions, as well as any views or opinions expressed herein, are those of the author(s) and do not necessarily reflect those of NOAA or the Department of Commerce.

REFERENCES

[1] E. M. A. S. Al-Ansari et al., "Seasonal variability of hydrography off the east coast of Qatar, Central Arabian Gulf," *Arabian J. Geosci.*, vol. 15, no. 22, Nov. 2022, Art. no. 1659.

[2] O. Lindeń et al., *State of the Marine Environment in the ROPME Sea Area (UNEP Regional Seas Reports and Studies)*. Nairobi, Kenya: UNEP, 1990.

[3] M. Al-Ansi, M. Abdel-Moati, and E. Al-Ansari, "Causes of fish mortality along the Qatari waters (Arabian Gulf)," *Int. J. Environ. Stud.*, vol. 59, pp. 59–71, Jan. 2002.

[4] E. M. A. S. Al-Ansari et al., "Hypoxia in the central Arabian Gulf exclusive economic zone (EEZ) of Qatar during summer season," *Estuarine, Coastal Shelf Sci.*, vol. 159, pp. 60–68, Jun. 2015.

[5] A. Al-Kaabi, H. Al-Sulaiti, T. Al-Ansari, and H. R. Mackey, "Assessment of water quality variations on pretreatment and environmental impacts of SWRO desalination," *Desalination*, vol. 500, Mar. 2021, Art. no. 114831.

[6] H. Hosseini et al., "Marine health of the Arabian Gulf: Drivers of pollution and assessment approaches focusing on desalination activities," *Mar. Pollut. Bull.*, vol. 164, Mar. 2021, Art. no. 112085.

[7] M. H. Bordbar, A. Nasrolahi, M. Lorenz, S. Moghaddam, and H. Burchard, "The Persian Gulf and Oman Sea: Climate variability and trends inferred from satellite observations," *Estuarine, Coastal Shelf Sci.*, vol. 296, Jan. 2024, Art. no. 108588.

[8] G. O. Vaughan, N. Al-Mansoori, and J. A. Burt, "Chapter 1–The Arabian Gulf," in *World Seas: An Environmental Evaluation*, 2nd ed., C. Sheppard, Ed. New York, NY, USA: Academic, 2019, pp. 1–23.

[9] F. Mirza Esmaeili, M. S. Mortazavi, A. Dehghan Banadaki, F. Saraji, and S. L. Mohebbi Nozar, "Algal blooms historical outbreaks in the northern coastal waters of the Persian Gulf and Oman Sea (1980–2015)," *Environ. Monit. Assessment*, vol. 193, no. 10, Sep. 2021, Art. no. 648.

[10] J. Zhao and H. Ghedira, "Monitoring red tide with satellite imagery and numerical models: A case study in the Arabian Gulf," *Mar. Pollut. Bull.*, vol. 79, no. 1, pp. 305–313, Feb. 2014.

[11] J. A. Al-Thani, Y. Soliman, I. A. Al-Maslamani, O. Yigiterhan, and E. M. A. S. Al-Ansari, "Physical drivers of chlorophyll and nutrients variability in the Southern-Central Arabian Gulf," *Estuarine, Coastal Shelf Sci.*, vol. 283, Apr. 2023, Art. no. 108260.

[12] F. Al Senafi, "Atmosphere-ocean coupled variability in the Arabian/Persian Gulf," *Front. Mar. Sci.*, vol. 9, Feb. 2022, Art. no. 809355.

[13] J. Shi and C. Hu, "South Florida estuaries are warming faster than global oceans," *Environ. Res. Lett.*, vol. 18, no. 1, 2023, Art. no. 014003.

[14] Z. Lachkar, M. Mehari, M. Lévy, F. Paparella, and J. A. Burt, "Recent expansion and intensification of hypoxia in the Arabian Gulf and its drivers," *Front. Mar. Sci.*, vol. 9, Sep. 2022, Art. no. 891378.

[15] A. Saleh et al., "Hypoxia in the Persian Gulf and the Strait of Hormuz," *Mar. Pollut. Bull.*, vol. 167, Jun. 2021, Art. no. 112354.

[16] M. Mannan, M. Alhaj, A. N. Mabrouk, and S. G. Al-Ghamdi, "Examining the life-cycle environmental impacts of desalination: A case study in the state of Qatar," *Desalination*, vol. 452, pp. 238–246, Feb. 2019.

[17] R. Sheikholeslami and S. Tan, "Effects of water quality on silica fouling of desalination plants," *Desalination*, vol. 126, no. 1, pp. 267–280, Nov. 1999.

[18] M. Omerspahic, H. Al-Jabri, S. A. Siddiqui, and I. Saadaoui, "Characteristics of desalination brine and its impacts on marine chemistry and health, with emphasis on the Persian/Arabian Gulf: A review," *Front. Mar. Sci.*, vol. 9, Apr. 2022, Art. no. 845113.

[19] D. A. Roberts, E. L. Johnston, and N. A. Knott, "Impacts of desalination plant discharges on the marine environment: A critical review of published studies," *Water Res.*, vol. 44, no. 18, pp. 5117–5128, Oct. 2010.

[20] T. Ben Hassen and H. El Bilali, "Sustainable agriculture and food security in Qatar: International threats and local constraints," in *Sustainable Agriculture and Food Security*, W. Leal Filho, M. Kovaleva, and E. Popkova, Eds. Berlin, Germany: Springer, 2022, pp. 425–442.

[21] A. Quigg et al., "Phytoplankton along the coastal shelf of an oligotrophic hypersaline environment in a semi-enclosed marginal sea: Qatar (Arabian Gulf)," *Continental Shelf Res.*, vol. 60, pp. 1–16, Jun. 2013.

[22] F. Rakib et al., "Observed variability in physical and biogeochemical parameters in the central Arabian Gulf," *Oceanologia*, vol. 63, no. 2, pp. 227–237, Apr. 2021.

[23] E. A. Elobaid, E. M. A. S. Al-Ansari, O. Yigiterhan, V. M. Aboobacker, and P. Vethamony, "Spatial variability of summer hydrography in the Central Arabian Gulf," *Oceanologia*, vol. 64, no. 1, pp. 75–87, Jan. 2022.

[24] M. Ghaemi, G. Mohammadpour, S. Hamzei, and S. Gholamipour, "Spatial and temporal characterizations of seawater quality on marine waters area of the Persian Gulf," *Regional Stud. Mar. Sci.*, vol. 53, Jun. 2022, Art. no. 102407.

[25] N. P. Nezlin, I. G. Polikarpov, F. Y. Al-Yamani, D. V. Subba Rao, and A. M. Ignatov, "Satellite monitoring of climatic factors regulating phytoplankton variability in the Arabian (Persian) Gulf," *J. Mar. Syst.*, vol. 82, no. 1, pp. 47–60, Jul. 2010.

[26] M. Zoljoodi, M. Moradi, and N. Moradi, "Seasonal and interannual cycles of total phytoplankton phenology metrics in the Persian Gulf using ocean color remote sensing," *Continental Shelf Res.*, vol. 237, Mar. 2022, Art. no. 104685.

[27] M. R. Al Kaabi, J. Zhao, and H. Ghedira, "MODIS-based mapping of Secchi disk depth using a qualitative algorithm in the shallow Arabian Gulf," *Remote Sens.*, vol. 8, no. 5, 2016, Art. no. 423.

[28] J. Zhao, M. Temimi, and H. Ghedira, "Characterization of harmful algal blooms (HABs) in the Arabian Gulf and the Sea of Oman using MERIS fluorescence data," *ISPRS J. Photogramm. Remote Sens.*, vol. 101, pp. 125–136, Mar. 2015.

[29] I. Polikarpov, F. Al-Yamani, and M. Saburova, "Remote sensing of phytoplankton variability in the Arabian/Persian Gulf," in *Remote Sensing of the Asian Seas*, V. Barale and M. Gade, Eds. Berlin, Germany: Springer, 2019, pp. 485–501.

[30] M. Moradi, "Trend analysis and variations of sea surface temperature and chlorophyll-a in the Persian Gulf," *Mar. Pollut. Bull.*, vol. 156, Jul. 2020, Art. no. 111267.

[31] Z. Chen, C. Hu, and F. Muller-Karger, "Monitoring turbidity in Tampa Bay using MODIS/Aqua 250-m imagery," *Remote Sens. Environ.*, vol. 109, no. 2, pp. 207–220, Jul. 2007.

[32] C. Hu, "A novel ocean color index to detect floating algae in the global oceans," *Remote Sens. Environ.*, vol. 113, no. 10, pp. 2118–2129, Oct. 2009.

[33] L. I. McKinna and P. J. Werdell, "Approach for identifying optically shallow pixels when processing ocean-color imagery," *Opt. Exp.*, vol. 26, no. 22, pp. A915–A928, 2018.

[34] C. C. Walton, W. G. Pichel, J. F. Sapper, and D. A. May, "The development and operational application of nonlinear algorithms for the measurement of sea surface temperatures with the NOAA polar-orbiting environmental satellites," *J. Geophysical Res., Oceans*, vol. 103, no. C12, pp. 27999–28012, 1998.

[35] C. Hu, Z. Lee, and B. Franz, "Chlorophyll a algorithms for oligotrophic oceans: A novel approach based on three-band reflectance difference," *J. Geophysical Res., Oceans*, vol. 117, no. C1, 2012, Art. no. C01011.

[36] A. I. Dogliotti, K. Ruddick, B. Nechad, D. Doxaran, and E. Knaeps, "A single algorithm to retrieve turbidity from remotely-sensed data in all coastal and estuarine waters," *Remote Sens. Environ.*, vol. 156, pp. 157–168, 2015.

[37] Z. Lee et al., "Secchi disk depth: A new theory and mechanistic model for underwater visibility," *Remote Sens. Environ.*, vol. 169, pp. 139–149, 2015.
[38] K. A. Kilpatrick et al., "A decade of sea surface temperature from MODIS," *Remote Sens. Environ.*, vol. 165, pp. 27–41, Aug. 2015.
[39] J. E. O'Reilly and P. J. Werdell, "Chlorophyll algorithms for ocean color sensors—OC4, OC5 and OC6," *Remote Sens. Environ.*, vol. 229, pp. 32–47, Aug. 2019.
[40] L. Qi, M. Wang, C. Hu, and B. Holt, "On the capacity of Sentinel-1 synthetic aperture radar in detecting floating macroalgae and other floating matters," *Remote Sens. Environ.*, vol. 280, Oct. 2022, Art. no. 113188.
[41] L. Qi, M. Wang, and C. Hu, "Uncertainties in MODIS-derived ulva prolifera amounts in the Yellow Sea: A systematic evaluation using Sentinel-2/MSI observations," *IEEE Geosci. Remote Sens. Lett.*, vol. 20, May 2023, Art. no. 1501805.
[42] F. Mélin, V. Vantrepotte, A. Chuprin, M. Grant, T. Jackson, and S. Sathyendranath, "Assessing the fitness-for-purpose of satellite multi-mission ocean color climate data records: A protocol applied to OC-CCI chlorophyll-a data," *Remote Sens. Environ.*, vol. 203, pp. 139–151, Dec. 2017.
[43] J. Laliberté and P. Larouche, "Chlorophyll-a concentration climatology, phenology, and trends in the optically complex waters of the St. Lawrence Estuary and Gulf," *J. Mar. Syst.*, vol. 238, Feb. 2023, Art. no. 103830.
[44] J. Xiang et al., "Evaluating the effectiveness of coastal environmental management policies in China: The case of Bohai Sea," *J. Environ. Manage.*, vol. 338, Jul. 2023, Art. no. 117812.
[45] S. Constantin, D. Doxaran, and Ş. Constantinescu, "Estimation of water turbidity and analysis of its spatio-temporal variability in the Danube River plume (Black Sea) using MODIS satellite data," *Continental Shelf Res.*, vol. 112, pp. 14–30, Jan. 2016.
[46] GEBCO Bathymetric Compilation Group, "The GEBCO_2020 grid—A continuous terrain model of the global oceans and land," Brit. Oceanogr. Data Centre, Nat. Oceanogr. Centre, NERC, Liverpool, U.K., 2020.
[47] L. M. Fanning et al., "Applying the ecosystem services—EBM framework to sustainably manage Qatar's coral reefs and seagrass beds," *Ocean Coastal Manage.*, vol. 205, May 2021, Art. no. 105566.
[48] S. Aljenaid et al., "Integrating remote sensing and field survey to map shallow water benthic habitat for the Kingdom of Bahrain," *J. Environ. Sci. Eng. B*, vol. 6, pp. 176–200, 2017.
[49] J. D. Butler, S. J. Purkis, R. Yousif, I. Al-Shaikh, and C. Warren, "A high-resolution remotely sensed benthic habitat map of the Qatari coastal zone," *Mar. Pollut. Bull.*, vol. 160, Nov. 2020, Art. no. 111634.
[50] T. V. Joydas et al., "Status of macrobenthic communities in the hypersaline waters of the Gulf of Salwa, Arabian Gulf," *J. Sea Res.*, vol. 99, pp. 34–46, May 2015.
[51] V. Aboobacker, S. Samiksha, S. Veerasingam, E. M. Al-Ansari, and P. Vethamony, "Role of Shamal and easterly winds on the wave characteristics off Qatar, Central Arabian Gulf," *Ocean Eng.*, vol. 236, 2021, Art. no. 109457.
[52] V. Aboobacker, P. Shanas, E. M. Al-Ansari, V. Sanil Kumar, and P. Vethamony, "The maxima in northerly wind speeds and wave heights over the Arabian Sea, the Arabian/Persian Gulf and the Red Sea derived from 40 years of ERA5 data," *Climate Dyn.*, vol. 56, pp. 1037–1052, 2021.
[53] V. M. Aboobacker, P. R. Shanas, S. Veerasingam, E. M. Al-Ansari, F. N. Sadooni, and P. Vethamony, "Long-term assessment of onshore and offshore wind energy potentials of Qatar," *Energies*, vol. 14, no. 4, 2021, Art. no. 1178.
[54] Z. Lee, K. L. Carder, C. D. Mobley, R. G. Steward, and J. S. Patch, "Hyperspectral remote sensing for shallow waters: 2—Deriving bottom depths and water properties by optimization," *Appl. Opt.*, vol. 38, no. 18, pp. 3831–3843, Jun. 1999.
[55] C. Hu, B. B. Barnes, L. Feng, M. Wang, and L. Jiang, "On the interplay between ocean color data quality and data quantity: Impacts of quality control flags," *IEEE Geosci. Remote Sens. Lett.*, vol. 17, no. 5, pp. 745–749, May 2020.
[56] L. Qi et al., "In search of floating algae and other organisms in global oceans and lakes," *Remote Sens. Environ.*, vol. 239, Mar. 2020, Art. no. 111659.
[57] L. Qi et al., "Trichodesmium around Australia: A view from space," *Geophysical Res. Lett.*, vol. 50, no. 16, 2023, Art. no. e2023GL104092.
[58] S. Seabold and J. Perktold, "statsmodels: Econometric and statistical modeling with python," in *Proc. 9th Python Sci. Conf.*, 2010, pp. 92–96.
[59] K. H. Hamed and A. R. Rao, "A modified Mann-Kendall trend test for autocorrelated data," *J. Hydrol.*, vol. 204, no. 1/4, pp. 182–196, 1998.
[60] P. K. Sen, "Estimates of the regression coefficient based on Kendall's Tau," *J. Amer. Stat. Assoc.*, vol. 63, no. 324, pp. 1379–1389, Dec. 1968.
[61] H. Ershadifar, A. Saleh, E. Koochaknejad, K. Kor, and A. Ghazilou, "Spatial and seasonal distribution of particulate phosphorous and nitrogen in the Persian Gulf: Nitrogen enrichment ties to diazotroph bloom in stratified warm waters," *Mar. Chem.*, vol. 253, Jun. 2023, Art. no. 104280.
[62] K. R. Ghadikolaei, "Quantitative (chlorophyll-a) and qualitative (species composition) seasonal fluctuations of phytoplankton in Lavan coastal waters (North of the Persian Gulf)," *Iranian J. Fisheries Sci.*, vol. 3, no. 2, pp. 109–119, 2001.
[63] S. A. Piontkovski et al., "Seasonal blooms of the dinoflagellate algae noctiluca scintillans: Regional and global scale aspects," *Regional Stud. Mar. Sci.*, vol. 44, May 2021, Art. no. 101771.
[64] M. Hamdeno, H. Nagy, O. Ibrahim, and B. Mohamed, "Responses of satellite chlorophyll-a to the extreme sea surface temperatures over the Arabian and Omani Gulf," *Remote Sens.*, vol. 14, no. 18, 2022, Art. no. 4653.
[65] C. C. C. Wabnitz et al., "Climate change impacts on marine biodiversity, fisheries and society in the Arabian Gulf," *PLoS One*, vol. 13, no. 5, 2018, Art. no. e0194537.
[66] P. M. Glibert et al., "Vulnerability of coastal ecosystems to changes in harmful algal bloom distribution in response to climate change: Projections based on model analysis," *Glob. Change Biol.*, vol. 20, no. 12, pp. 3845–3858, 2014.
[67] H. A. Naser, "Marine ecosystem diversity in the Arabian Gulf: Threats and conservation," in *Biodiversity*, G. Oscar, Ed. Rijeka, Croatia: IntechOpen, 2014, pp. 297–328.
[68] C. Hu et al., "Building an automated integrated observing system to detect sea surface temperature anomaly events in the Florida keys," *IEEE Trans. Geosci. Remote Sens.*, vol. 47, no. 6, pp. 1607–1620, Jun. 2009.
[69] J. Wei, X. Yu, Z. Lee, M. Wang, and L. Jiang, "Improving low-quality satellite remote sensing reflectance at blue bands over coastal and inland waters," *Remote Sens. Environ.*, vol. 250, 2020, Art. no. 112029.
[70] N. Al-Naimi, D. E. Raitsos, R. Ben-Hamadou, and Y. Soliman, "Evaluation of satellite retrievals of chlorophyll-a in the Arabian Gulf," *Remote Sens.*, vol. 9, no. 3, 2017, Art. no. 301.
[71] J. Wei, Z. Lee, and S. Shang, "A system to measure the data quality of spectral remote-sensing reflectance of aquatic environments," *J. Geophysical Res., Oceans*, vol. 121, no. 11, pp. 8189–8207, 2016.
[72] W. Javed and B. Guo, "Chemical characterization and source apportionment of fine and coarse atmospheric particulate matter in Doha, Qatar," *Atmos. Pollut. Res.*, vol. 12, no. 2, pp. 122–136, Feb. 2021.
[73] A. Al-Hemoud et al., "Dust storm 'hot spots' and transport pathways affecting the Arabian Peninsula," *J. Atmos. Sol.-Terr. Phys.*, vol. 238/239, Nov. 2022, Art. no. 105932.

Cheng Xue received the B.S. degree in physics from the Ocean University of China, Qingdao, China, in 2016, and the Ph.D. degree in marine detection technology (ocean optics and ocean color remote sensing) from the Ocean University of China, Qingdao, in 2022.

He is currently a Postdoctoral Scholar with the Optical Oceanography Laboratory, College of Marine Science, University of South Florida, St. Petersburg, FL, USA. His research interests include in-situ observation for water optical properties, ocean color algorithm development, and the application of satellite radiometric data to the aquatic environment.

Chuanmin Hu received the B.S. degree in physics from the University of Science and Technology of China, Hefei, China, in 1989, and the Ph.D. degree in physics (environmental optics) from the University of Miami, Coral Gables, FL, USA, in 1997.

He is currently a Professor of optical oceanography with the University of South Florida, St. Petersburg, FL, and also directs the Optical Oceanography Laboratory. He uses laboratory, field, and remote sensing techniques to study marine algal blooms (harmful and nonharmful, macroalgae, and microalgae), oil spills, coastal and inland water quality, and global changes.

Dr. Hu was a Topical Editor on ocean optics and ocean color remote sensing of *Applied Optics* from 2009 to 2014. From 2015 to 2017, he was a Chief Editor of *Remote Sensing of Environment*.

Jennifer P. Cannizzaro received the B.A. degree in biology from Mount Holyoke College, South Hadley, MA, USA, in 1993, and the M.S. degree in marine science from the University of South Florida, St. Petersburg, FL, USA, in 2004.

She is currently a Research Scientist with the Optical Oceanography Laboratory, College of Marine Science, University of South Florida. Her research focuses on developing remote sensing algorithms for monitoring harmful algal blooms using satellite ocean color data.

Brian B. Barnes received the B.S. degree in zoology and psychology from the University of Florida, Gainesville, FL, USA, in 2004, the M.S. degree in marine science from the College of William and Mary, Virginia Institute of Marine Science, Gloucester Point, VA, USA, in 2009, and the Ph.D. degree in marine science from the University of South Florida, St. Petersburg, FL, in 2013.

He is currently a Research Assistant Professor with the Optical Oceanography Laboratory, College of Marine Science, University of South Florida. His research interests include improving satellite retrievals in optically complex environments, calibration and validation of ocean color satellite data, assessing continuity of satellites for ocean color research, and floating matter characterization.

Lin Qi received the B.S. degree in geography information system (GIS) from the East China University of Technology, Fuzhou, China, in 2008, the M.S. degree in GIS from Nanjing Normal University, Nanjing, China, in 2011, and the Ph.D. degree in remote sensing and GIS from the Nanjing Institute of Geography and Limnology, Chinese Academy of Sciences, Nanjing, in 2015.

She is currently a Research Scientist with the NOAA Ocean Color Science Team. Her research interests include optical characterization and remote sensing of floating macroalgae, phytoplankton, and organic matters in global oceans and lakes, and their responses to climate variability and human activities.

Jing Shi received the B.S. degree in geographical information system from Hunan Normal University, Changsha, China, in 2015, and the M.S. degree in cartography and geography information system from Nanjing University, Nanjing, China, in 2019. She is currently working toward the Ph.D. degree in optical oceanography with the University of South Florida, St. Petersburg, FL, USA.

Her research focuses on assessing water temperature changes in coastal and inland waters, to analyze the potential impacts of temperature changes on seagrasses.

Yuyuan Xie received the B.S. and Ph.D. degrees in marine science from the Xiamen University, Xiamen, China, in 2007 and 2015, respectively.

He is currently a Research Scientist with the Optical Oceanography Laboratory, College of Marine Science, University of South Florida, St. Petersburg, FL, USA. His research focuses on the phytoplankton functional types in relation to marine primary production.

Benjamin D. Jaffe received a B.A. degree in animal behavior from Franklin and Marshall College, Lancaster, PA, USA, in 2003, the M.A. degree in behavioral ecology from the University of Chicago, Chicago, IL, USA, in 2006, and the Ph.D. degree in biological sciences from Northern Arizona University, Flagstaff, AZ, USA, in 2015.

He was a Postdoctoral Researcher in chemical ecology with the United States Department of Agriculture from 2015 to 2016, and with the University of Wisconsin-Madison, Madison, WI, USA, from 2016 to 2019. He then worked as an Applied Ecologist with ExxonMobil Biomedical Sciences, Inc., Annandale, NJ, USA, from 2019 to 2023. Since 2023, he has been a Technical Lead with ExxonMobil Research Qatar's Center for Nature-based Solutions, Doha, Qatar, focusing on sustainable land management and biodiversity monitoring. His research interests include quantification of cobenefits associated with nature-based solutions and improving efficiency and accuracy of biodiversity monitoring.

David A. Palandro (Member, IEEE) received the B.S. degree in biology and history from the from the State University of New York, Brockport, NY, USA, in 1993, the M.S. and Ph.D. degrees in marine science from the University of South Florida, St. Petersburg, FL, USA, in 2000 and 2006, respectively.

He is currently the Vice President and Research Director of ExxonMobil Research Qatar, Doha, Qatar, where he was the Global Principal for Marine Environmental Management and Chief on the Global Emergency Response Team. He was a Research Scientist and Scientific Support Coordinator for Oil Spill Response for the Florida Fish and Wildlife Conservation Commission.

Dr. Palandro is a Member of the International Coral Reef Society.